

Brazil Malvinas Frontal System as seen from 9 years of advanced very high resolution radiometer data

Martín Saraceno,¹ Christine Provost,¹ Alberto R. Piola,^{2,3}
José Bava,⁴ and Antonio Gagliardini⁴

Received 18 September 2003; revised 30 December 2003; accepted 22 March 2004; published 25 May 2004.

[1] Surface thermal fronts in the southwestern Atlantic (SWA) Ocean are examined using 9 years (1987–1995) of advanced very high resolution radiometer data. Fronts are detected considering a gradient based edge detector. Sea surface temperature gradients are calculated from 4 km resolution 5-day composite images covering the western Argentine Basin south of 30°S. Variability in the position and intensity of the fronts from seasonal to interannual timescales is characterized in six regions including different parts of the Brazil Current Front (BCF) and the Subantarctic Front (SAF): Shelf Break-Brazil (SB-B), Brazil Malvinas Collision (BM-C), Brazil Current-Overshoot (BC-O), Shelf Break-Malvinas (SB-M), Malvinas Return Flow (MRF), and Falkland Escarpment (FE). Fronts in the SB-B, SB-M, MRF, and FE regions are controlled by the bathymetry. In the BM-C region the BCF and SAF appear to merge as a single front. This front does not present large seasonal north-south excursions as previously described, though it pivots seasonally around a fixed point located approximately at 39.5°S, 53.5°W, changing its orientation from N-S in winter to NW-SE in summer. Consequently, on average, the front intersects the 1000 m isobath at 38°30'S in summer and north of 37°S in winter. In the BC-O region the BCF has a U-shape centered at 53°W. The intensity of the fronts in each region except in the FE region presents large seasonal variability. In the SB-B, BM-C, and BC-O regions the frontal intensity is highest ($>0.35^{\circ}\text{C}/\text{km}$) during austral winter, the annual components explain 83, 67, and 71% of the total variance, respectively. In the SB-M and MRF regions the SAF is most intense ($>0.25^{\circ}\text{C}/\text{km}$) in summer and fall; the annual component of the intensity fluctuations explains 29 and 38% of the total variance, respectively. In the FE region the annual component of frontal intensity explains only 17% of the variability. In the six regions, important interannual variability is found. The Zapiola Rise (centered at 45°S, 43°W) appears as a gradient-free region. Closed planetary potential vorticity contours in this area suggest it is dynamically isolated. INDEX TERMS: 4223 Oceanography: General: Descriptive and regional oceanography; 4520 Oceanography: Physical: Eddies and mesoscale processes; 4528 Oceanography: Physical: Fronts and jets; KEYWORDS: southwest Atlantic, sea surface temperature fronts, Brazil Malvinas Conference

Citation: Saraceno, M., C. Provost, A. R. Piola, J. Bava, and A. Gagliardini (2004), Brazil Malvinas Frontal System as seen from 9 years of advanced very high resolution radiometer data, *J. Geophys. Res.*, 109, C05027, doi:10.1029/2003JC002127.

1. Introduction

[2] Frontal regions are key oceanic features both for the biological activity and for the climate at regional and global scales. Frontal regions are characterized by pronounced horizontal gradients and are generally associated to enhanced

exchanges between the ocean and the atmosphere and to a stronger vertical circulation in the ocean. These two processes have an important impact on the biomass [Froneman *et al.*, 1997; Brandini *et al.*, 2000; Olson, 2000] and on the rates at which gases are exchanged with the atmosphere.

[3] The southwest Atlantic is a region where the circulation generates numerous strong fronts. The Malvinas Current (MC) and the Brazil Current (BC) collide near 38°S forming the Brazil/Malvinas Confluence region (BMC, hereafter), one of the most energetic regions of the world ocean [Chelton *et al.*, 1990; Gordon, 1981]. A general circulation scheme of the region is shown in Figure 1. The MC is part of the northern branch of the Antarctic Circumpolar Current (ACC) [Piola and Gordon, 1989] that carries the cold ($<7^{\circ}\text{C}$ at the surface in winter) and relatively fresh Subantarctic Mode Water (SAMW) equatorward along the western edge of the Argentine Basin. The BC flows

¹Laboratoire d'Océanographie Dynamique et de Climatologie, Université Pierre et Marie Curie, Paris, France.

²Departamento de Oceanografía, Servicio de Hidrografía Naval, Buenos Aires, Argentina.

³Also at Departamento de Ciencias de la Atmósfera y los Océanos, Facultad de Ciencias Exactas y Naturales, Universidad de Buenos Aires, Buenos Aires, Argentina.

⁴Instituto de Astronomía y Física del Espacio, Ciudad Universitaria, Buenos Aires, Argentina.

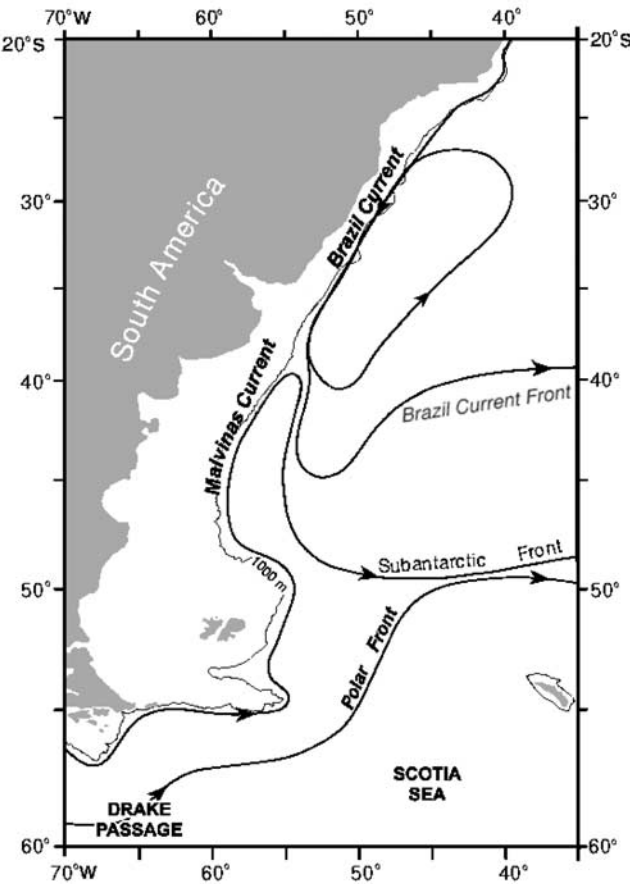


Figure 1. Schematic diagram of the upper layer circulation in the SWA (based on Brandini *et al.* [2000] and Peterson and Stramma [1990]).

poleward along the continental margin of South America as part of the western boundary current of the South Atlantic subtropical gyre. It transports the warm (higher than 26°C at the surface) and salty South Atlantic Central Water (SACW).

[4] After its confluence with the MC, the BC separates in two branches. One branch turns to the north forming a recirculation cell while the other branch flows southward and returns to the northeast at about 45°S. The second branch is referred to as the overshoot of the Brazil Current and, east of 45°W, it forms the South Atlantic Current [Peterson and Stramma, 1990].

[5] After the collision with the BC the main flow of the MC describes a sharp loop forming the Malvinas return flow. The Malvinas return flow flows southward and turns to the east at 49°S.

[6] Advanced very high radiometer resolution (AVHRR) images reveal the sea surface temperature (SST) patterns associated with the upper layer currents in the SWA. In particular, the AVHRR images clearly show the strong surface thermal gradients associated with frontal regions.

[7] In the SWA two strong oceanic fronts are present: the Brazil Current Front (BCF) and the Subantarctic Front (SAF), which are the objective of this study. The BCF is the southern limit of the SACW, while the SAF is the northernmost front within the ACC [Peterson and

Whitworth, 1989] and is the northern limit of the recently ventilated SAMW in the western South Atlantic [Piola and Gordon, 1989; Peterson, 1992].

[8] In the literature most of the attention is devoted to the study of the BCF, which presents the highest mesoscale variability in the BMC zone. Two distinct parameters are used to study the variability of the position of the BCF: its separation from the continental margin and the southernmost position of the overshoot. Using AVHRR data from 1981 to 1987, Olson *et al.* [1988] estimated that the BC separates from the 1000 m isobath around 36.5°S while using a combination of altimeter and thermocline depth data, Goni and Wainer [2001] found that in the period 1993–1998 the separation occurs, on average, at $38.5 \pm 0.8^{\circ}\text{S}$. Using less than 2 years of VHRR data Legeckis and Gordon [1982] found that the southern limit of the BC overshoot fluctuates between 38 and 46°S, with a timescale of 2 months; a similar result was found by Goni and Wainer [2001]. Tracing isotherms on SST images Olson *et al.* [1988] estimated that the SAF separates from the continental shelf break at $38.6 \pm 0.9^{\circ}\text{S}$, that is two degrees to the south of the Brazil Current separation point. They found that the range of migration of the separation point for the BC and MC is of ~ 900 km, which is quite large relative to other boundary current systems. The observed timescale of variability ranges from 30–60 days to semiannual and annual scales, with important interannual variability.

[9] In this study we use an objective method to describe the variability of the position and intensity of the thermal fronts present in the SWA based on 9 years of AVHRR data. This is the longest time series of high spatial resolution (4×4 km) AVHRR data used to study the frontal variability in the western South Atlantic. This allows us to better establish the seasonal and lower frequencies and evaluate the interannual variability in the position and intensity of the fronts.

[10] The paper is organized as follows: in section 2 we present the data and methods, and the subregions used in the rest of the paper are defined; results are described in section 3; finally, discussion and a synthesis of the main results are presented in section 4.

2. Data and Methods

[11] The satellite-derived SST observations were obtained from the advanced very high resolution radiometer (AVHRR) onboard NOAA-N polar orbital satellites (NOAA-7 to NOAA-13 in the present case). The SST time series here analyzed spans 9 years from January 1987 to December 1995, and consists of 633 5-day composite images with approximately a 4×4 km resolution. The data processing, including cloud detection and 5-day compositing, was performed at the Rosenstiel School of Marine and Atmospheric Science, University of Miami (RSMAS) and is described in the work of Olson *et al.* [1988] and Podesta *et al.* [1991]. Use of 5-day composites reduces the effect of cloud coverage and the likelihood of negative biases due to cloud contamination [Podesta *et al.*, 1991]. The remaining seasonal cloud cover is shown on Figure 2. Cloud cover is lowest in austral summer and highest in winter, autumn and spring present intermediate cloudiness

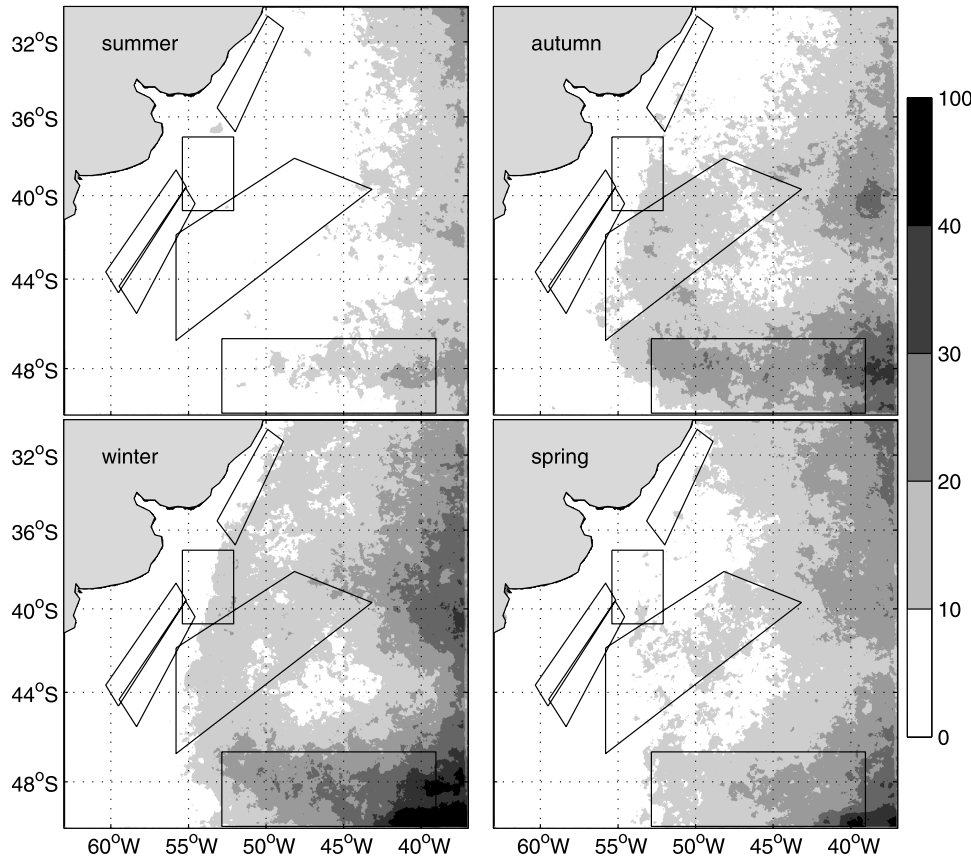


Figure 2. Seasonal probability of the cloudy pixels for the period 1987–1995 considering the AVHRR data described in the text. Dark pixels correspond to regions with higher probability of cloudiness. Boxes represent the different regions studied (see definitions in the text and Figure 3).

values. Spatially, cloud coverage presents a similar pattern throughout the year: it is higher in the east of the region and south of 46°S. The continental shelf has a remarkably low cloud coverage (<10% for all seasons). In general for a given location the difference between summer and winter cloud cover is lower than 10%. Similar spatiotemporal cloudiness pattern in the SWA was described by *Escoffier and Provost* [1998]. On the basis of the low differences in cloud cover between seasons described above, we consider that frontal characteristics (defined further in this section) are not affected by the seasonal cloud cover variability.

[12] The front detection can be treated as an edge detection problem. Edge detection is one of the basic components of image analysis techniques. Different edge detectors have been developed, mostly as a discrete approximation to the gradient. Local gradient operators use fixed threshold to distinguish an edge from background values. A usual criticism to gradient-based edge detectors is that they are characterized by a spurious response when applied to noisy data. A different technique was developed by *Cayula and Cornillon* [1992]: instead of computing gradients they use the bimodality of the histogram in a local window as the basic edge detector. The resulting edge detection is based not on the absolute strength of the front gradient but on the separability of pixel values to different compact areas.

[13] Comparing gradient and histogram based edge detectors to in situ observations *Ullman and Cornillon* [2000]

estimate two types of errors. Error rates associated to false front detection are lower for the histogram method, while missed fronts associated to error rates are lower for the gradient method.

[14] In the present work we use a gradient based edge detector which uses the separability of the gradient pixel values based on the cumulative histogram of the gradient pixels. As will be shown, the gradient images are not noisy, and a threshold based on the cumulative histogram rather than a fixed value accommodates for the time variations. This criterion is commonly used for edge detection in digital image processing techniques [*Wolfram*, 2003] but to our knowledge, this is the first time that such an approach is applied to detect SST fronts.

[15] For each SST composite the gradient magnitude is calculated using centered differences as:

$$\|\text{grad}(\text{SST}(i))\| = \sqrt{\left(\frac{\text{SST}(ix+1) - \text{SST}(ix-1)}{\text{dist}(ix+1, ix-1)}\right)^2 + \left(\frac{\text{SST}(iy+1) - \text{SST}(iy-1)}{\text{dist}(iy+1, iy-1)}\right)^2}, \quad (1)$$

where $ix-1$ and $ix+1$ ($iy-1$ and $iy+1$) are the neighbors of the i th pixel in the X (Y) direction; dist is the distance in the X (Y) direction.

[16] The 9-year mean SST gradient distribution is presented on Figure 3. The mean positions of the SAF and BCF

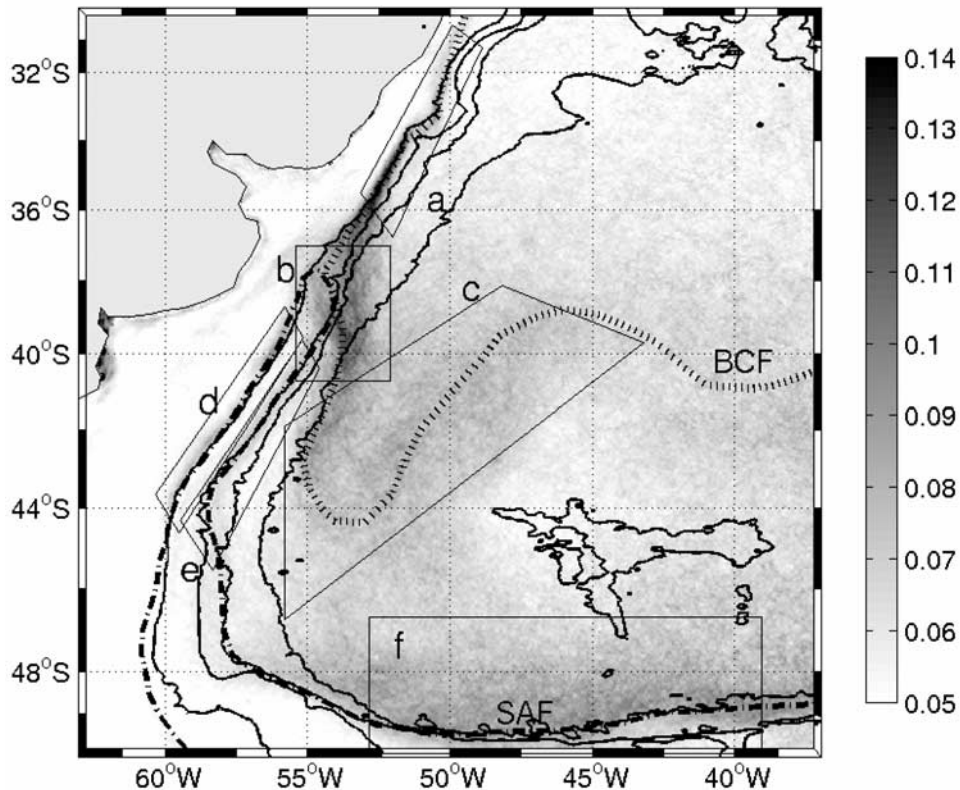


Figure 3. Average of the norm of the SST gradient magnitude (in $^{\circ}\text{C}/\text{km}$) for the period 1987–1995. The mean positions of the Subantarctic Front (dash-dot line) and of the Brazil Current Front (dot line) are plotted considering the maximum gradient values. Letters identify the studied regions: (a) Shelf Break-Brazil, (b) Brazil Malvinas-Collision, (c) Brazil Current-Overshoot, (d) Shelf Break-Malvinas, (e) Malvinas return flow, and (f) Falkland Escarpment. Thin black lines from west to east correspond to the 2×10^{-7} , 5×10^{-8} , 3×10^{-8} , $2 \times 10^{-8} \text{ m}^{-1} \text{ s}^{-1}$ potential vorticity (f/h) contours, respectively; obtained from *Smith and Sandwell [1994]* bathymetry. These contours roughly coincide with the 300, 2000, 3000 and 4500 m isobaths, respectively. See color version of this figure at back of this issue.

are easily identified and can be compared to the schematic circulation shown in Figure 1. Figure 1 is a mixed schematic representation of currents and fronts, whereas Figure 3 shows the thermal fronts which are located at the boundaries of the Malvinas and Brazil Currents.

[17] Seasonal variability differs considerably from front to front. For example, the intensity of the western part of the BCF is lowest in summer and highest in winter, while the western part of the SAF is stronger in late summer and weaker in winter. To discern the different time and space variations of each part of the BCF and SAF we define six regions (marked by letters “a” to “f” in Figure 3), that we shall examine separately:

[18] 1. The Shelf Break-Brazil (SB-B) region includes the western part of the BCF, located between 31 and 36°S; it separates shelf waters off Brazil and Uruguay from the SACW carried southward by the BC; the 9 years mean highest values in this region reach $0.13^{\circ}\text{C}/\text{km}$.

[19] 2. The Brazil/Malvinas Collision (BM-C) region extends from 37°S to 41°S and from 53 to 55.5°W, highest mean gradient values are $0.12^{\circ}\text{C}/\text{km}$.

[20] 3. The Brazil Current Overshoot (BC-O) region includes the southern limit of the BC after the collision

with the MC. The BCF in this region reaches its southernmost position. The region extends from 38°S–45°W to 46.5°S–55°W. The highest SST gradient value in this region is $0.08^{\circ}\text{C}/\text{km}$.

[21] 4. The Shelf Break-Malvinas (SB-M) region includes the western part of the SAF located between 39 and 44°S. Maximum mean gradients here reach $0.07^{\circ}\text{C}/\text{km}$.

[22] 5. The Malvinas/Return Flow (MRF) region includes part of the SAF and is roughly parallel to the SB-M region. It marks the eastern boundary of the Malvinas current. Mean maximum gradients in the MRF reach $0.07^{\circ}\text{C}/\text{km}$.

[23] 6. The Falkland Escarpment (FE) region is located around 48°S and between 39 and 53°W and includes the eastern part of the SAF. The highest mean SST gradient is $0.1^{\circ}\text{C}/\text{km}$.

[24] To examine the variability of the position and intensity of the fronts we calculate two indices on each of the six different regions described above: (1) the most probable position of the fronts, and (2) a time series of the frontal intensities. Both indices are based on the SST gradient derived from the AVHRR data. We first identify frontal pixels within each region from each of the 633 SST gradient

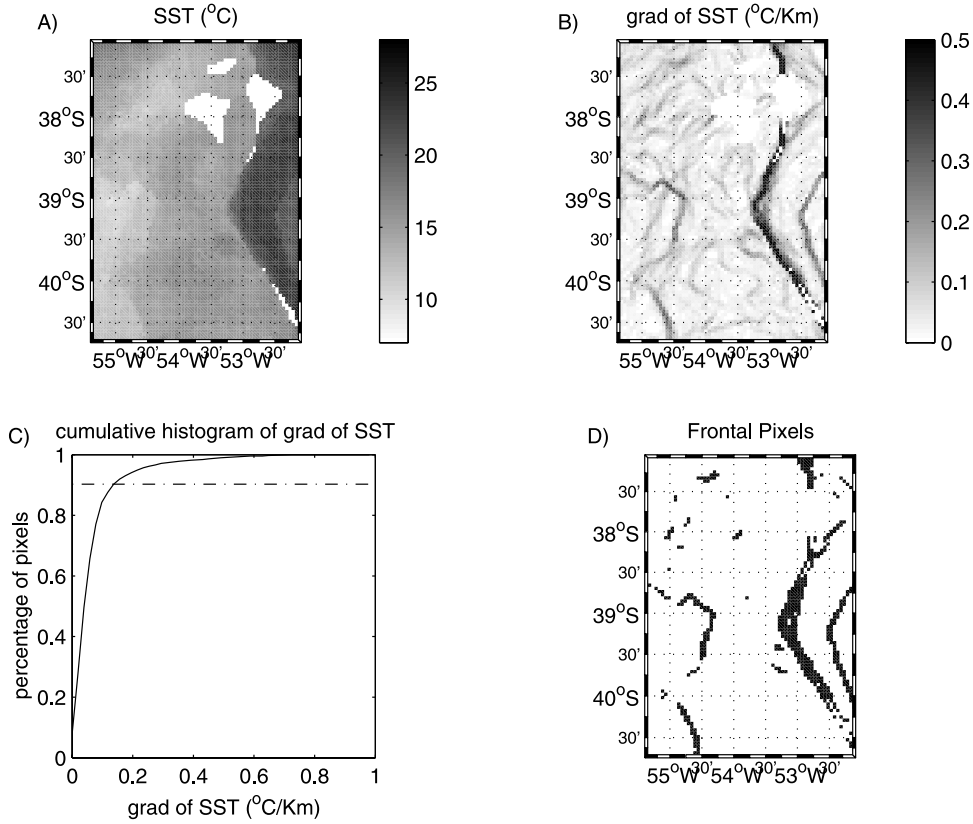


Figure 4. (a) SST (in $^{\circ}$ C) for the BM-C region for the 5-day composite centered on 16 December 1995. (b) SST gradient ($^{\circ}$ C/km). (c) Bold line, cumulative histogram of the SST gradient; dash-dotted line, maximum curvature of the cumulative histogram. (d) Frontal pixel values according to the percentage associated to the maximum curvature of the cumulative histogram.

images. To distinguish frontal pixels (edges) from background values we examine the cumulative histogram of the gradient values.

[25] For clarity we illustrate in Figures 4a–4d the edge detection process for one image in the BM-C region. Figure 4a shows four different masses of water, corresponding in the figure to different levels of gray. The western part corresponds to cold water ($\sim 10^{\circ}$ C) probably advected by the MC, while along $53^{\circ}30'W$ there is warm water (24° C) advected by the BC. The norm of the SST gradient (Figure 4b) clearly shows the edges between the different water masses (dark values correspond to gradients greater than 0.2° C/km); a number of secondary (less intense) fronts are also detected. The cumulative histogram of the gradient image (Figure 4c) allows us to classify pixels in two categories: a large percentage of pixels with low gradient values (background or frontless pixels) and a small percentage with the highest gradient values (frontal pixels). To separate the two categories we use the point of maximum curvature in the cumulative histogram curve. The maximum curvature point corresponds to a percentage of 91% on Figure 4c (dashed line), that is 91% of the pixels are background values and 9% are frontal pixels. Figure 4d shows that the frontal pixels selected do correspond to the major fronts observed in Figure 4b.

[26] The procedure described above to select frontal pixels was repeated for each of the 633 SST gradient images. Figure 5 shows how the percentage corresponding

to the maximum curvature of the cumulative histogram varies with time between 0.92 (8% frontal pixels) and 0.83 (17% frontal pixels). Using the maximum curvature of the cumulative histogram to select frontal pixels for each figure avoids spurious front detection. Thus seasonal average of frontal probability maps and time intensity series (see definitions below) results are less contaminated than if they were obtained using a fixed threshold. The time series display a high frequency resolution superimposed over a seasonal signal. High percentages of frontal pixels selected are present in winter.

[27] In each region the frontal pixels, selected as described above, are used to study the variability of frontal location and intensity:

[28] 1. To study the variability in the position of the fronts we assign a one to the frontal pixels, zero to the remaining noncloud pixels, and not-a-number (NaN) to the cloudy pixels. Frontal probability maps are then obtained by averaging in time these new images. Frontal probability values vary between 0 and 1.

[29] 2. To study the variability of frontal intensity within a region the SST gradient of all frontal pixels are averaged at each time step and a time series is constructed.

[30] If at one time the cloud cover exceeds 50% of the surface of a given region, data for that time and that region is not considered. The number of gaps thus produced varies between 5 to 9% for all regions except for the FE, where the number of gaps reaches 20% of the total time series.

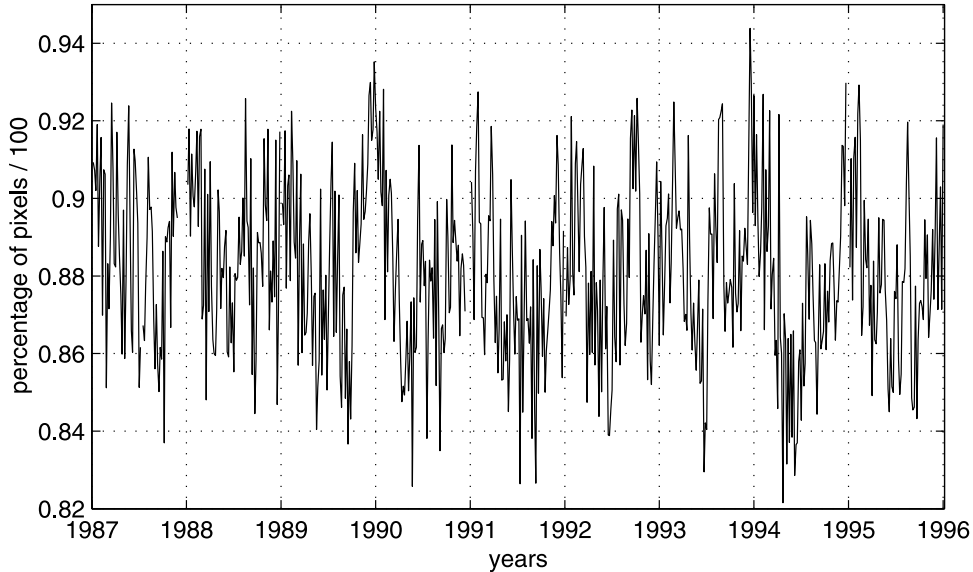


Figure 5. Time series of the percentage of frontless pixels for the BM-C region determined from the maximum curvature point of the cumulative histogram on each SST gradient image.

[31] In order to calculate spectra of the time series, gaps are filled using a cubic spline interpolation. Spectra, confidence limits (CL) and significant peaks of the time series are then calculated using the singular spectrum analysis-multitaper method (SSA-MTM) toolkit [Ghil *et al.*, 2002]. We configure the SSA-MTM toolkit to work with the multitaper method [Thomson, 1982; Percival and Walden, 1993] using three data tapers. Significant peaks have been estimated with the hypothesis of a harmonic process drawn back in a background red noise. The variance explained by each significant peak is computed as:

$$\text{explained variance} = \left(1 - \left(\frac{\text{var}(S - F)}{\text{var}(S)} \right)^2 \right), \quad (2)$$

where S is the original series, F the best fit to S in the least squares sense considering the analyzed frequency and var is the variance.

[32] Frequency resolution of the spectral estimation is estimated as $2pf_n$ where p is an integer determined by the number of data tapers used [Percival and Walden, 1993] and f_n is the Rayleigh frequency. The resulting frequency resolution is 0.0006 days^{-1} .

[33] The position of the fronts is confronted to planetary potential vorticity isolines. As long as dissipation and other external vorticity sources remain small, barotropic and equivalent-barotropic flows tend to conserve angular momentum by following lines of constant potential vorticity $(f + z)/h$, where F is the planetary vorticity, z is the relative vorticity and h is the ocean depth. In open ocean areas planetary vorticity is generally larger than relative vorticity, and potential vorticity can be approximated by the planetary potential vorticity f/h . Planetary potential vorticity contours have been used in a similar approach by Moore *et al.* [1997] in studying how the Polar Front is controlled by topography in the SWA.

[34] To select which contours of f/h to compare to the frontal positions we calculated the gradient of the bathym-

etry (not shown), and then selected the f/h contours that best fitted the maximum gradients of the bathymetry. These maxima are located at the edge of the South American continental shelf. The f/h contours represented in Figure 3 and in the following figures roughly correspond to the 300, 2000, 3000 and 4500 m isobaths.

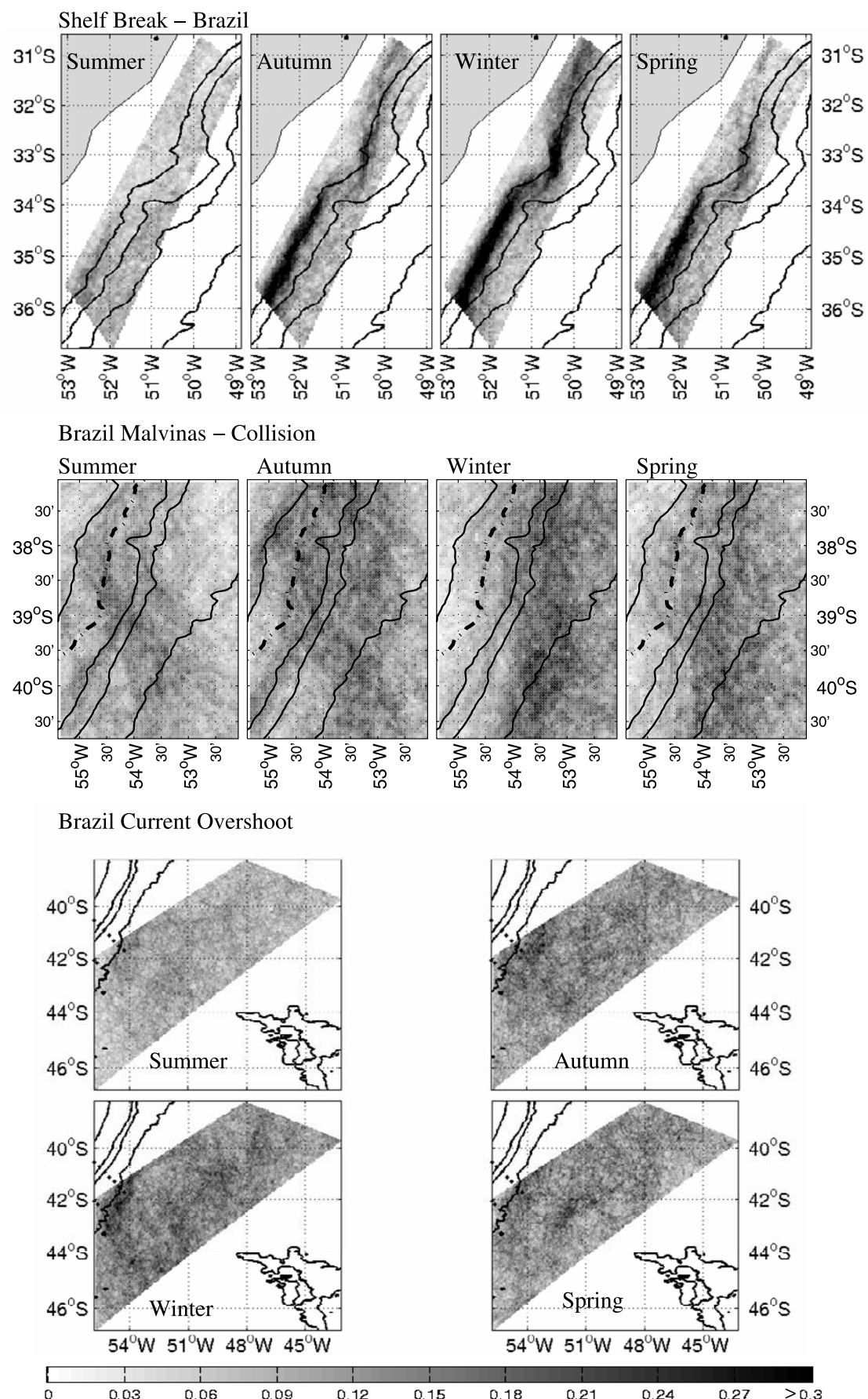
3. Results

[35] The seasonal frontal probability maps and the time series of the intensity of the fronts are analyzed within each of the regions defined earlier. The results obtained for each region are presented in Figures 6, 7, 8, 9, 10, and 11 and are described in this section. Throughout the rest of the article, summer and winter values are means over January–February–March and July–August–September respectively, i.e., austral seasons.

3.1. Shelf Break-Brazil Region

[36] The frontal probability values in the SB-B region (Figure 6) clearly show the position of the BCF. The probability is highest in winter (values up to 0.5) and lowest in summer (<0.18). South of 32°S the frontal location in winter, spring and autumn closely follows the $f/h = 2 \times 10^{-7} \text{ m}^{-1} \text{ s}^{-1}$ contour (roughly the 300 m isobath). This indicates that the BC closely follows the western boundary, as expected. However, north of 32°S in autumn, winter and spring the surface front is observed further onshore, suggesting that Brazil Current waters often occupies the shelf there. In agreement with this observation, based on surface temperature and salinity distributions a southward intrusion of tropical waters by an inshore branch of the Brazil Current during the Austral winter has been suggested [Castro and Miranda, 1998]. In summer the probability is distributed more homogeneously south of 34°S and is lower to the north.

[37] The frontal intensity (Figure 7) exhibits large annual amplitude with low values in summer and high values in winter. The crest-valley difference is not constant in time and it is as large as $0.35^\circ\text{C}/\text{km}$ between summer and winter

**Figure 6**

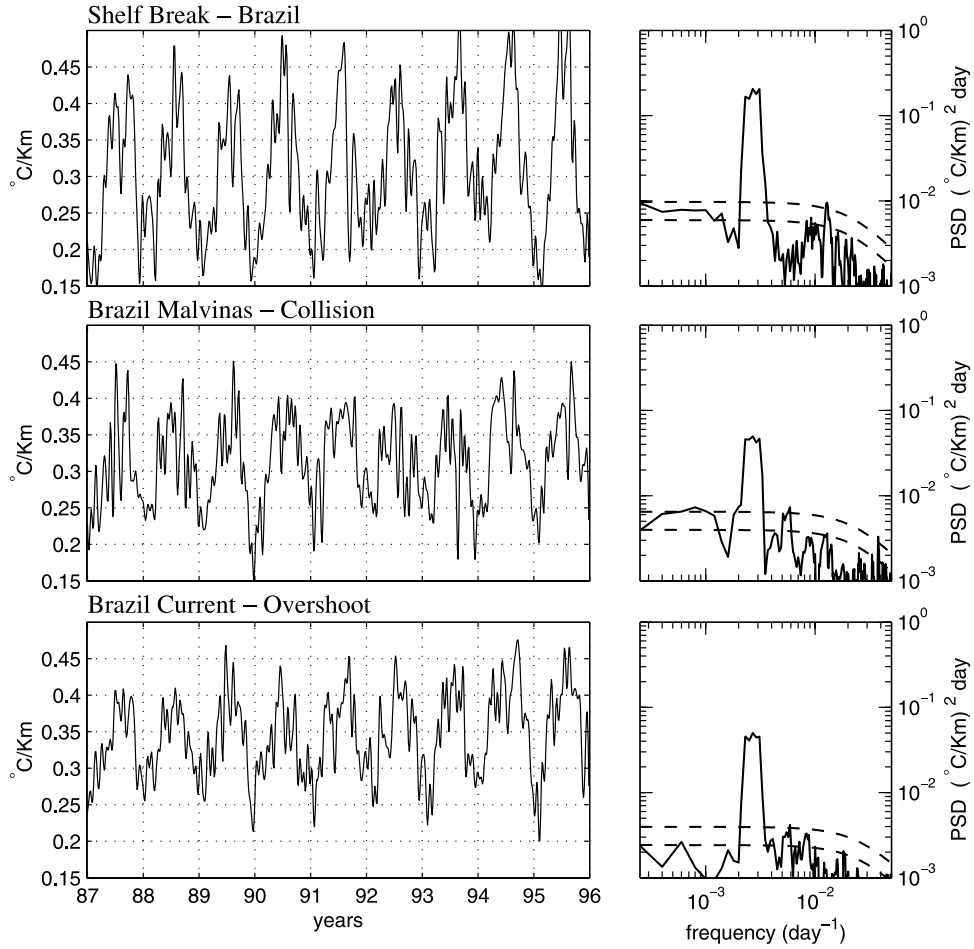


Figure 7. (top) Frontal intensity time series and power spectral density for the Shelf Break-Brazil region, (middle) Brazil Malvinas Collision region, and (bottom) Brazil Current Overshoot region. Dashed lines in spectra indicate 90 and 99% confidence levels.

of 1995. The mean intensity value is $0.31^{\circ}\text{C}/\text{km}$. The annual signal (99% CL) explains 83% of the variability of the frontal intensity (Figure 7).

[38] East of the front, the BC transports warm water southward throughout the year, and presents relatively small seasonal SST variations. In contrast, over the shelf and west of the front, enhanced northward advection of relatively cold waters occurs in winter [Piola et al., 2000], inducing a high seasonal SST amplitude. Thus increased cross-front SST gradients are observed in winter. In addition, in summer a thin and sharp seasonal thermocline develops leading to similar SST values across the front. Consequently, in summer the intensity of the front decreases and its position is not well-defined.

3.2. Brazil Malvinas Collision Region

[39] On average, in the period 1987–1995 we observe a single front corresponding to the collision between the BC and the MC and not two distinct fronts as described in the past

[Olson et al., 1988]. The front pivots seasonally, around a fixed point located approximately at $39^{\circ}30'\text{S}$, $53^{\circ}30'\text{W}$. In winter the front is orientated N-S along $53^{\circ}30'\text{W}$, while in summer the highest frontal location probability is observed between 38 and 40°S with a NW-SE direction (Figure 6). As a result of this pivoting, the front intersects the 1000 m isobath at $38^{\circ}30'\text{S}$ in summer, whereas in winter the intersection occurs out of our domain, north of 37°S .

[40] The frontal probability marks a precise orientation in summer and winter. However, in autumn and spring the frontal probability values are distributed more homogeneously, front positions are intermediate between the summer and winter positions.

[41] The power spectrum of the frontal intensity time series (Figure 7) reveals three peaks. The annual peak (99% CL) explains 67% of the variance. The semiannual peak (99%CL) has the largest amplitude of the six time series studied, relative to the annual peak. The interannual variability present in the time series leads to a peak centered at

Figure 6. (top) Seasonal frontal probability distribution for the Shelf Break-Brazil region, (middle) Brazil Malvinas Collision region, and (bottom) Brazil Current Overshoot region. Solid black lines are the f/h contours indicated in Figure 3. Dash-dotted line in the BM-C region is the 1000 m isobath. The color bar indicates the frontal probability and is common for all panels. See color version of this figure at back of this issue.

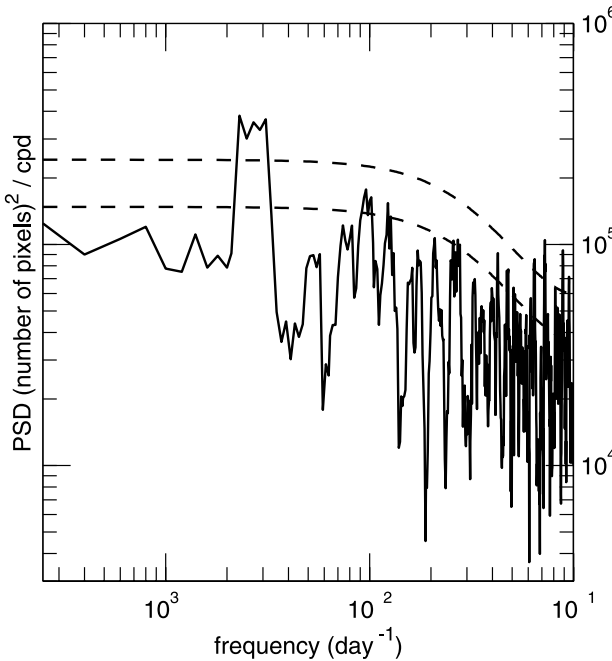


Figure 8. Power spectrum density (PSD) of the number of frontal pixels observed south of 44°S, in the BC-O region. Units for PSD are (number of pixels)²/cpd, where cpd is cycles per day. Dashed lines in spectra indicate 90 and 99% confidence levels.

3.4 years (99%CL). However, the spectral amplitude at interannual timescales is not well-resolved by the 9-year time series. As in the SB-B region, the thin and strong seasonal thermocline that develops in summer is responsible for the seasonality in the frontal intensity and the low probability values presents in summer.

3.3. Brazil Current-Overshoot Region

[42] Frontal probability values in the BC-O region (Figure 6) are nearly homogeneously distributed in each season, reflecting the high spatial variability of the BCF in this region. The BCF marks in this region the southern limit of the BC after it collides with the MC. In all seasons but summer the BCF has a U-shape centered at 53°W. This U path is known in the literature as the overshoot of the BC. According to the seasonal frontal probability maps the BCF southernmost position is reached in winter (45°S). Frontal probability values are higher in autumn, winter and spring. Lower values in summer are due to the seasonal thermocline that develops in the region, which masks the subsurface structure and homogenizes the SST values.

[43] The intensity of the front (Figure 7) presents a strong annual peak (99% CL) that explains 71% of the variability. Low values are present in summer and higher values in winter. Winter values reveal a slight trend: $0.0053 \pm 0.0013^\circ\text{C}/\text{km/year}$. Two additional peaks centered on the semiannual (99% CL) and 4-month (95% CL) periods are observed.

[44] To further investigate the meridional excursions of the BCF we calculate a time series of the number of frontal pixels detected in this region that are south of 44°S. The associated spectrum (Figure 8) shows a strong peak cen-

tered near the annual period (99% CL) and two other peaks at 104 ± 7 days (95% CL) and at 81 ± 4 days (90% CL) that reflects the timescales associated with the meridional excursions of the overshoot. Similar timescales in the displacements of the Brazil Current overshoot were observed by Legeckis and Gordon [1982].

3.4. Shelf Break-Malvinas and Malvinas Return Flow Regions

[45] The corresponding portions of the SAF in the SB-M and MRF regions are roughly parallel. The SAF in the SB-M region separate shelf waters from the MC while the SAF in the MRF region separate the MC from the Malvinas return flow.

[46] The probability of presence of the SAF in both regions (Figure 9) is higher in summer and autumn and lower in winter and spring. In both regions the bathymetry controls the position of the front.

[47] In the SB-M region the front closely follows the $f/h = 2 \times 10^{-7} \text{ m}^{-1} \text{ s}^{-1}$ contour (300 m isobath): the probability rises from zero in frontless areas to up to 30% in the frontal region. In winter values of up to 12% occur east of the $f/h = 2 \times 10^{-7} \text{ m}^{-1} \text{ s}^{-1}$ contour. In autumn the front breaks into a northern and southern part at 41°S.

[48] In the MRF region the frontal probability is distributed more homogeneously. In summer and autumn the SAF more probable position follows the $f/h = 5 \times 10^{-8} \text{ m}^{-1} \text{ s}^{-1}$ contour (2000 m depth). High values in the NE edge of the region are associated to the BCF. The bottom slope is less steep south of 43°S, leading to a weaker topographic control and allowing larger frontal excursions.

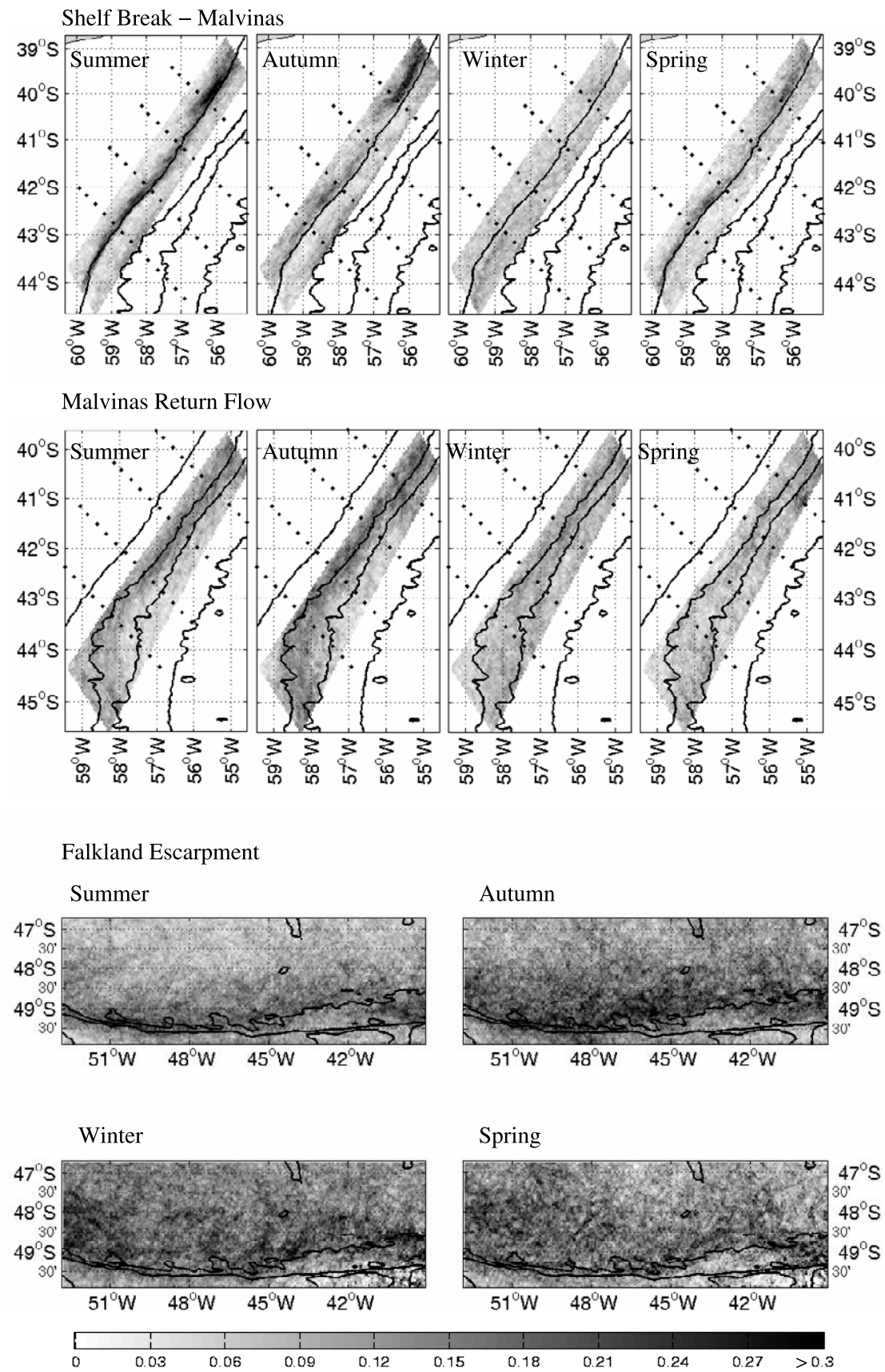
[49] The frontal intensity time series in both regions (Figure 10) share some properties. Both series present interannual variability, for instance, frontal intensity is high in 1994 and low in 1995. Higher values are observed in summer and autumn than in winter and spring and both spectra show a strong annual component (99% CL) that explains 29% and 38% of the variability for the SB-M and MRF respectively.

[50] The MC transports cold water northward throughout the year, and presents relatively small seasonal SST variations [Podesta et al., 1991; Provost et al., 1992]. In contrast, high seasonal SST amplitude occurs over the shelf and east of the MC [Podesta et al., 1991; Provost et al., 1992]. The major difference between the SST amplitudes occurs in autumn and summer, leading to increased cross-front SST gradients in those seasons east and west of the MC.

[51] The seasonality of the SAF is summarized in Figure 11. We extract the gradient time series from four sections orthogonal to the f/h contours which include both SB-M and MRF regions (see Figure 9). The seasonal average shows maximum gradients around the f/h contours detected in the seasonal frontal probability maps. The highest SAF intensity is observed in summer in the SB-M region and in autumn in the MRF region (Figure 11). Lowest SAF gradients are found in winter at the SB-M region and in winter and spring at the MRF region. High gradient values in the eastern part of these sections correspond to the presence of the BC.

3.5. Falkland Escarpment Region

[52] High frontal probability values (>0.25) are widely distributed in the FE region in autumn, winter and spring

**Figure 9**

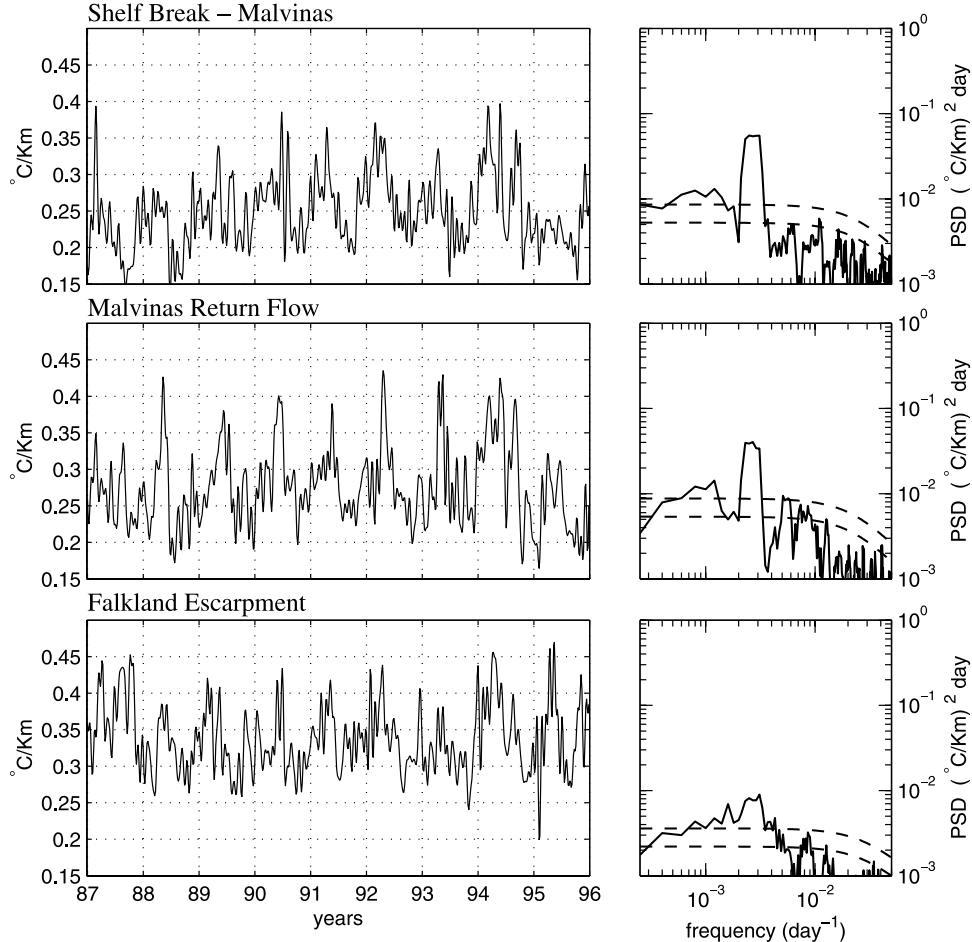


Figure 10. (top) Frontal intensity time series and power spectral density for the Shelf Break-Malvinas region, (middle) Malvinas Return Flow region, and (bottom) Falkland Escarpment region. Dashed lines in spectra indicate 90 and 99% confidence levels.

(Figure 9). In summer a narrow band of high values is observed closely following the $f/h = 2 \times 10^{-8} \text{ m}^{-1} \text{ s}^{-1}$ contour ($\sim 4500 \text{ m}$ depth). This contour is a well-defined southern limit for the high probability throughout the year. The wide distribution of high probability values in this region could be associated to the presence of eddies from the BMC region: in summer the SST increases and consequently the gradient associated to the presence of warm eddies is lower. The narrow band present in summer is associated to the mean position of the SAF. The larger cloud cover observed in this region can be a factor that introduces a bias on the frontal probability maps.

[53] The frontal intensity time series (Figure 10) shows large interannual variability: crest-valley differences vary from year to year. As in the SB-M and MRF regions, 1994

is anomalously high. Consequently, the annual cycle (99% CL) accounts only for 17% of the observed variability.

4. Discussion

4.1. Position of the Fronts: Influence of the Bathymetry

[54] The mean SST gradient (Figure 3) clearly shows the fronts located at the boundaries of the Malvinas and Brazil Currents. The boundaries of the MC are represented by the SAF in the SB-M region (western boundary) and in the MRF region (eastern boundary) that follows the 300 and 2000 m isobaths, respectively. The core of the MC follows the 1000 m isobath [Vivier and Provost, 1999a]. The northern limit of the MC establishes the front in the BM-C region. East of the SAF in the MRF region the Malvinas return flow flows southward.

Figure 9. (top) Seasonal frontal probability distribution for the Shelf Break-Malvinas region, (middle) Malvinas Return Flow region, and (bottom) Falkland Escarpment region. Solid black lines are the f/h contours indicated in Figure 3. Dots in upper and middle panels indicate the locations selected to study the cross-front structure presented in Figure 11. On each section points are separated by $\sim 30 \text{ km}$. The color bar indicates the frontal probability (and is common for all panels). Frontal probability values ranges from 0 to 1. See color version of this figure at back of this issue.

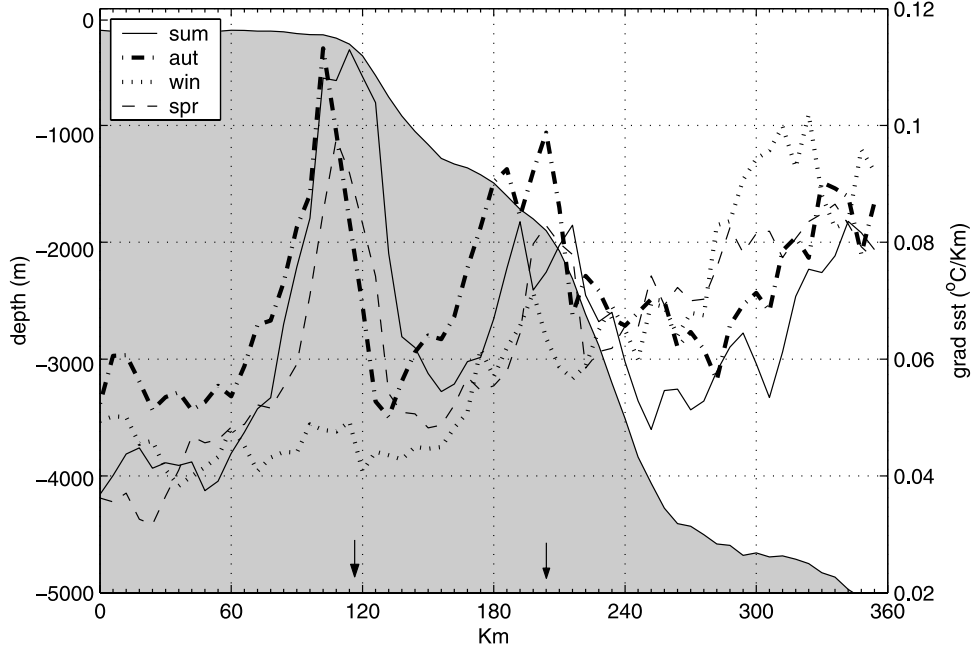


Figure 11. Mean SST gradient from the northern section displayed in Figure 9. The section is orthogonal to the f/h contours. Because similar results are found on the four sections, only the northern one is shown here. The bathymetry is displayed in the shaded background. The arrows in the x axis indicate the position where the planetary vorticity is $2 \times 10^{-7} \text{ m}^{-1} \text{ s}^{-1}$ ($\sim 300 \text{ m}$ depth) and $5 \times 10^{-8} \text{ m}^{-1} \text{ s}^{-1}$ ($\sim 2000 \text{ m}$ depth) $\text{m}^{-1} \text{ s}^{-1}$ from left to right, respectively.

[55] The mean position of the SAF and BCF closely follow contours of constant potential vorticity in the following regions:

[56] 1. The front in the SB-B region is trapped by the $f/h = 2 \times 10^{-7} \text{ m}^{-1} \text{ s}^{-1}$ contour (300 m depth) south of 32°S . The deep thermocline of the BC [Maamaatuiaahutapu *et al.*, 1992] is presumably responsible for the topographic control in this region. In winter, north of 32°S the BCF is found onshore of the f/h contour probably due to the influence of an inshore branch of the Brazil Current observed during the Austral winter [Castro and Miranda, 1998].

[57] 2. The SAF in the SB-M region is also trapped by the $f/h = 2 \times 10^{-7} \text{ m}^{-1} \text{ s}^{-1}$ contour (300 m depth). The equivalent-barotropic structure of the MC [Vivier and Provost, 1999b] is likely responsible for linking the frontal location to the f/h contour.

[58] 3. The collision of the Brazil and Malvinas currents forces the resulting jet to leave the continental margin. The BCF in the collision and overshoot regions is not controlled by the topography.

[59] 4. Once the MC collides with the BC, it flows southward forming the Malvinas return flow. The SAF is the western edge of the Malvinas return flow in this region. The SAF in the MRF region follows the $f/h = 5 \times 10^{-8} \text{ m}^{-1} \text{ s}^{-1}$ contour (2000 m depth) and therefore also seems to be subject to topographic control.

[60] Different authors assign different extents to the region of separation of the SAF and the BCF at the BMC region (Figure 1) [Peterson and Stramma, 1990; Olson *et al.*, 1988]. Indeed the difficulty in determining the frontal positions is due to the strong mesoscale activity present in this region. On the basis of the calculation of the SST

gradients we find evidence that, on average, only one well-defined front is present. The front pivots seasonally, around a fixed point located around 39.5°S , 53.5°W . In winter the front is orientated N-S along 53.5°W , while in summer the highest probability is found between 38 and 40°S with a NW-SE direction. Using a set of closely spaced hydrographic stations Provost *et al.* [1996] observed that the location of the surface temperature front in the summer of 1990 was not coincident with the location of the subsurface temperature structure which, at the time, had a north-south orientation, similar to that observed in winter in this study. Surface and 100 m temperature summer distributions from the World Ocean Database 2001 [Conkright *et al.*, 2002] show that in the BMC region the fronts have a different orientation at these levels (Figure 12). As observed by Provost *et al.* [1996] the summer isotherms have a NW-SE direction, while in winter they are oriented in a N-S direction. This suggests that the decoupling between the surface and subsurface thermal structure is the typical situation in summer. The strong and very shallow ($<20 \text{ m}$) seasonal thermocline that develops in summer may be responsible of the above mentioned decoupling [Provost *et al.*, 1996].

[61] The seasonal frontal displacement revealed by the frontal probability maps in the BM-C region (Figure 6) is also apparent in the 9-year annual mean gradient distribution (Figure 3). It is therefore possible to follow the winter position north of the BM-C region and check that it intersects the 1000 m isobath north of 37°S , approximately at $36^{\circ}30'\text{S}$. This is in good agreement with independent front location estimates based on a combination of satellite altimetry and hydrographic data [Goni and Wainer, 2001].

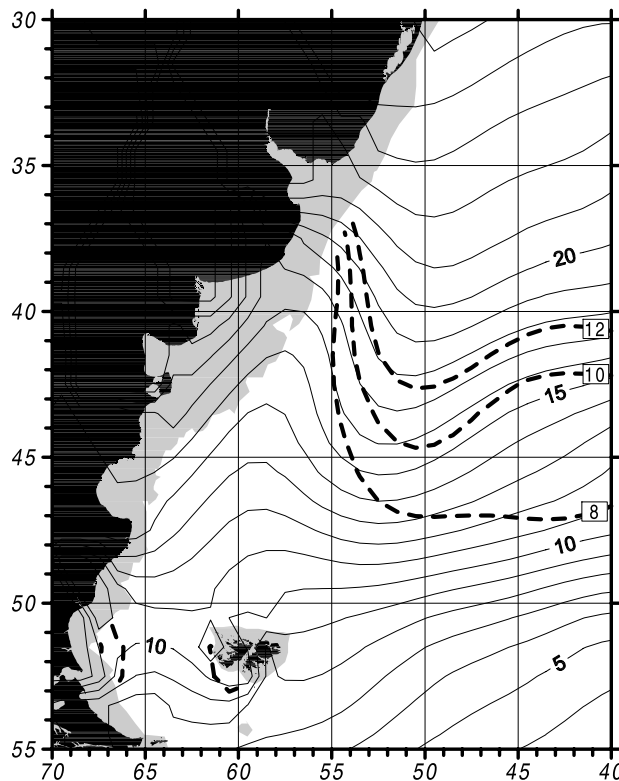


Figure 12. Mean summer sea surface temperature distribution (in °C) in the western South Atlantic prepared from the World Ocean Atlas 2001 [Conkright *et al.*, 2002]. The contour interval is 1°C. The heavy dashed lines are the summer 8, 10, and 12°C isotherm at 100 m depth. Shaded areas are shallower than 100 m.

[62] In the overshoot region the BCF has a U-shape and presents a meridional fluctuation with significant periodicities centered at one year (99% CL), 104 ± 7 days (95% CL) and at 81 ± 4 days (90% CL). The BCF southernmost position in this region is reached in winter (45° S). The 81-day periodicity and the southernmost position of the BCF in the region that we find are similar to those described by Legeckis and Gordon [1982]. More recently Goni and Wainer [2001] using altimeter-derived anomaly data obtained similar periodicities for the southernmost location of the BCF (at 60, 90, 180 and 360 days, significant at 85% CL) but a lower value for the mean southernmost position: 42.3° S.

[63] In Figure 3 the Zapiola Rise (centered approximately at 45° S, 43° W) appears as a gradient-free region, surrounded by the BCF to the north and the SAF to the south. Fu *et al.* [2001] suggested that the closed f/h contours provide a mechanism for the confinement of the waves associated to the topographic feature of the Zapiola Rise. They suggested a mass transport variability of the order of 50 Sv ($1\text{ Sv} = 10^6 \text{ m}^3 \text{ s}^{-1}$). The region is dynamically isolated and consequently corresponds to a region of low SST gradients.

4.2. Intensity of the Fronts: Dominance of the Annual Period

[64] The annual signal explains the greatest percentage of SST gradient frontal intensity time series in all regions. Except for the SB-M and MRF regions, frontal intensity time series present maximum values during austral winter.

The strong seasonal signal is likely due to the seasonal variations of solar radiation. The surface layer warming generates a strong and shallow seasonal thermocline that leads to a more uniform surface temperature distribution. Consequently, the horizontal temperature gradients are reduced in spring and summer. In contrast, in autumn and winter, convective overturning and wind mixing increase the mixed layer depth, and the surface temperature and the associated horizontal gradient are more representative of the subsurface temperature structure. In the SB-M and MRF regions others factors dominate the seasonal variability. The highest gradient intensity is reached in austral summer because the MC advects waters much colder than those present on the continental shelf [Rivas and Piola, 2002]. In winter the water on the continental shelf is almost as cold as in the MC, therefore in winter the SST gradient is lower than in summer. Thus both advection and sea-air heat fluxes are important in determining the SST gradients. Similar arguments have been used by Podesta *et al.* [1991] and by Legeckis and Gordon [1982] to explain the minimum in the gradient intensity of the SAF.

[65] The eastern side of the MRF region deserves special attention: here flows southward the Malvinas return flow, which is a mixture between the Malvinas and Brazil currents. Because of the presence of warm water advected by BC, one might expect a well-developed SAF in this region in winter. However, the winter SST reveals little temperature contrast with the MC. This could be due to the fact that the Malvinas return flow is located in a region of maximum winter heat loss to the atmosphere [Escoffier and Provost, 1998].

[66] Frontal intensity time series presents interannual variability in all regions. In particular we find that the SAF in the SB-M, MRF and FE regions present positive gradient anomalies in 1994.

[67] Our analysis of the variability in the position and intensity of the fronts is based on estimates of the gradient of the skin temperature obtained from satellite measurements. Our results are therefore only valid for the skin layer of the ocean. The advection of warm and cold waters by the BC and the MC into the Argentine Basin lead to the formation of a complex system of SST fronts. The intensity of these fronts presents significant seasonal variability associated to sea-air heat fluxes and horizontal advection. In addition, current meanders, eddies and filaments induce large space and time variability of the fronts, creating one of the most energetic eddy regions in the World Ocean. Here we have only examined these fronts based on their SST expression. Given the complexity of the region, a more complete insight of the frontal characteristics and variability will require the combined analysis of SST and other available satellite data (e.g., ocean color and sea-surface height).

[68] **Acknowledgments.** MS and JB are supported by fellowships from Consejo Nacional de Investigaciones Científicas y Técnicas (Argentina) and ARP by a Collaborative Research Network grant from the Inter-American Institute for Global Change Research and by the Agencia Nacional de Ciencia y Tecnología (Argentina) through grant PICT99 07-06420 BID 1201/OC-AR.

References

- Brandini, F. P., D. Boltovskoy, A. Piola, S. Kocmura, R. Rottgers, P. C. Abreu, and R. M. Lopes (2000), Multiannual trends in fronts and dis-

- tribution of nutrients and chlorophyll in the southwestern Atlantic (30–62°S), *Deep Sea Res., Part I*, 47, 1015–1033.
- Castro, B. M., and L. B. Miranda (1998), Physical oceanography of the western Atlantic continental shelf located between 4°N and 34°S, in *The Sea*, vol. 11, edited by A. R. Robinson and K. H. Brink, chap. 8, pp. 209–251, John Wiley, Hoboken, N. J.
- Cayula, J.-F., and P. C. Cornillon (1992), Edge detection algorithm for SST images, *J. Atmos. Oceanic Technol.*, 9(1), 67–80.
- Chelton, D. B., M. G. Schlax, D. L. Witter, and J. G. Richman (1990), GEOSAT altimeter observations of the surface circulation of the Southern Ocean, *J. Geophys. Res.*, 95, 17,877–17,903.
- Conkright, M. E., R. A. Locarnini, H. E. Garcia, T. D. O'Brien, T. P. Boyer, C. Stephens, and J. I. Antonov (2002), *World Ocean Atlas 2001: Objective Analyses, Data Statistics, and Figures* [CD-ROM], 17 pp., Natl. Oceanogr. Data Cent., Silver Spring, Md.
- Escoffier, C., and C. Provost (1998), Surface forcing over the southwest Atlantic according to NCEP and ECMWF reanalyses over the period 1979–1990, *Phys. Chem. Earth*, 23, 537–542.
- Froneman, P. W., R. Perissinotto, and E. A. Pakhomov (1997), Biogeographical structure of the microphytoplankton assemblages in the region of the subtropical convergence and across a warm-core eddy during austral winter, *J. Plankton Res.*, 19, 519–531.
- Fu, L.-L., B. Cheng, and B. Qiu (2001), 25-day period large-scale oscillations in the Argentine Basin revealed by the TOPEX/POSEIDON altimeter, *J. Phys. Oceanogr.*, 31, 506–517.
- Ghil, M., et al. (2002), Advanced spectral methods for climatic time series, *Rev. Geophys.*, 40(1), 1003, doi:10.1029/2000RG000092.
- Goni, G., and I. Wainer (2001), Investigation of the Brazil current front dynamics from altimeter data, *J. Geophys. Res.*, 106, 31,117–31,128.
- Gordon, A. L. (1981), South Atlantic thermocline ventilation, *Deep Sea Res.*, 28, 1239–1264.
- Legeckis, R., and A. Gordon (1982), Satellite observations of the Brazil and Falkland currents—1975 to 1976 and 1978, *Deep Sea Res.*, 29, 375–401.
- Maamaataiahutapu, K., V. Garçon, C. Provost, M. Boulahdid, and A. P. Osiroff (1992), Brazil-Malvinas confluence: Water mass composition, *J. Geophys. Res.*, 97, 9493–9505.
- Moore, J. K., M. R. Abbott, and J. G. Richman (1997), Variability in the location of the Antarctic Polar Front (90°–20°W) from satellite sea surface temperature data, *J. Geophys. Res.*, 102, 27,825–27,833.
- Olson, D. B. (2000), Biophysical dynamics of ocean fronts, in *The Sea*, vol. 12, chap. 5, edited by A. R. Robinson and K. H. Brink, pp. 187–218, John Wiley, Hoboken, N. J.
- Olson, D. B., G. P. Podesta, R. H. Evans, and O. B. Brown (1988), Temporal variations in the separation of Brazil and Malvinas currents, *Deep Sea Res.*, 35, 1971–1990.
- Percival, D. B., and A. T. Walden (1993), *Spectral Analysis for Physical Applications—Multitaper and Conventional Univariate Techniques*, 580 pp., Cambridge Univ. Press, New York.
- Peterson, R. G. (1992), The boundary currents in the western Argentine basin, *Deep Sea Res.*, 39, 623–644.
- Peterson, R. G., and L. Stramma (1990), Upper-level circulation in the South Atlantic Ocean, *Prog. Oceanogr.*, 26, 1–73.
- Peterson, R. G., and T. Whitworth III (1989), The sub-Antarctic and Polar Fronts in relation to deep water masses through the southwestern Atlantic, *J. Geophys. Res.*, 94, 10,817–10,838.
- Piola, A. R., and A. L. Gordon (1989), Intermediate water in the southwest South Atlantic, *Deep Sea Res.*, 36, 1–16.
- Piola, A. R., E. J. D. Campos, O. O. Moller Jr., M. Charo, and C. Martinez (2000), The Subtropical Shelf Front off eastern South America, *J. Geophys. Res.*, 105, 6565–6578.
- Podesta, G. P., O. B. Brown, and R. H. Evans (1991), The annual cycle of satellite-derived sea surface temperature in the southwestern Atlantic Ocean, *J. Clim.*, 4, 457–467.
- Provost, C., O. Garcia, and V. Garçon (1992), Analysis of satellite sea surface temperature time series in the Brazil-Malvinas Current confluence region: Dominance of the annual and semiannual periods, *J. Geophys. Res.*, 97, 17,841–17,858.
- Provost, C., V. Garçon, and L. M. Falcon (1996), Hydrographic conditions in the surface layers over the slope-open ocean transition area near the Brazil-Malvinas Confluence during austral summer 1990, *Cont. Shelf Res.*, 16, 215–235.
- Rivas, A. L., and A. R. Piola (2002), Vertical stratification at the shelf off northern Patagonia, *Cont. Shelf Res.*, 22, 1549–1558.
- Smith, W. H. F., and D. T. Sandwell (1994), Bathymetric prediction from dense satellite altimetry and sparse shipboard bathymetry, *J. Geophys. Res.*, 99, 21,803–21,824.
- Thomson, D. J. (1982), Spectrum estimation and harmonic analysis, *Proc. IEEE*, 70, 1055–1096.
- Ullman, D. S., and P. C. Cornillon (2000), Evaluation of front detection methods for satellite-derived SST data using in situ observations, *J. Atmos. Oceanic Technol.*, 17, 1667–1675.
- Vivier, F., and C. Provost (1999a), Direct velocity measurements in the Malvinas Current, *J. Geophys. Res.*, 104, 21,083–21,103.
- Vivier, F., and C. Provost (1999b), Volume transport of the Malvinas Current: Can the flow be monitored by TOPEX/POSEIDON?, *J. Geophys. Res.*, 104, 21,105–21,122.
- Wolfram, S. (2003), *The Mathematica Book*, 5th ed., Cambridge Univ. Press, New York.
-
- J. Bava and A. Gagliardini, Instituto de Astronomía y Física del Espacio, Ciudad Universitaria, C.C. 67 suc. 28, 1428 Buenos Aires, Argentina.
- A. R. Piola, Departamento de Oceanografía, Servicio de Hidrografía Naval, Av. Montes de Oca 2124, 1271 Buenos Aires, Argentina.
- C. Provost and M. Saraceno, Laboratoire d’Océanographie Dynamique et de Climatologie, Université Pierre et Marie Curie-Tour 45, Etage 5, Boite 100, 4 Place Jussieu, F-75252 Paris cedex 05, France. (martin.saraceno@odoc.jussieu.fr)

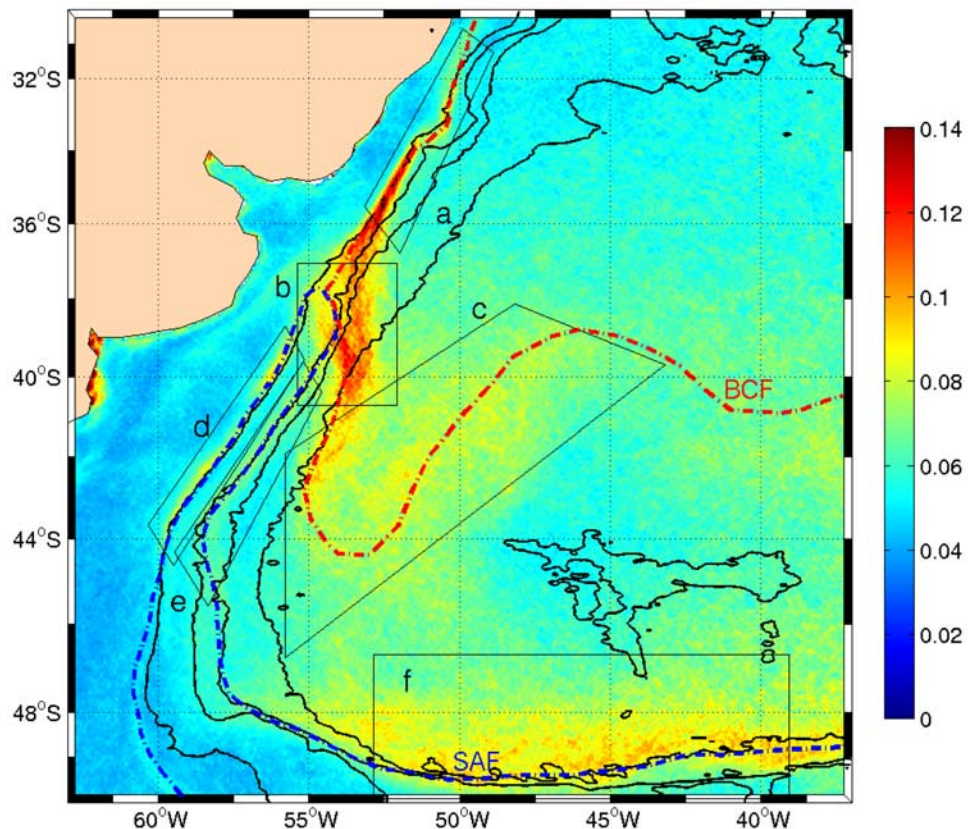


Figure 3. Average of the norm of the SST gradient magnitude (in $^{\circ}\text{C}/\text{km}$) for the period 1987–1995. The mean positions of the Subantarctic Front (dash-dot line) and of the Brazil Current Front (dot line) are plotted considering the maximum gradient values. Letters identify the studied regions: (a) Shelf Break-Brazil, (b) Brazil Malvinas-Collision, (c) Brazil Current-Overshoot, (d) Shelf Break-Malvinas, (e) Malvinas return flow, and (f) Falkland Escarpment. Thin black lines from west to east correspond to the 2×10^{-7} , 5×10^{-8} , 3×10^{-8} , $2 \times 10^{-8} \text{ m}^{-1} \text{ s}^{-1}$ potential vorticity (f/h) contours, respectively; obtained from *Smith and Sandwell [1994]* bathymetry. These contours roughly coincide with the 300, 2000, 3000 and 4500 m isobaths, respectively.

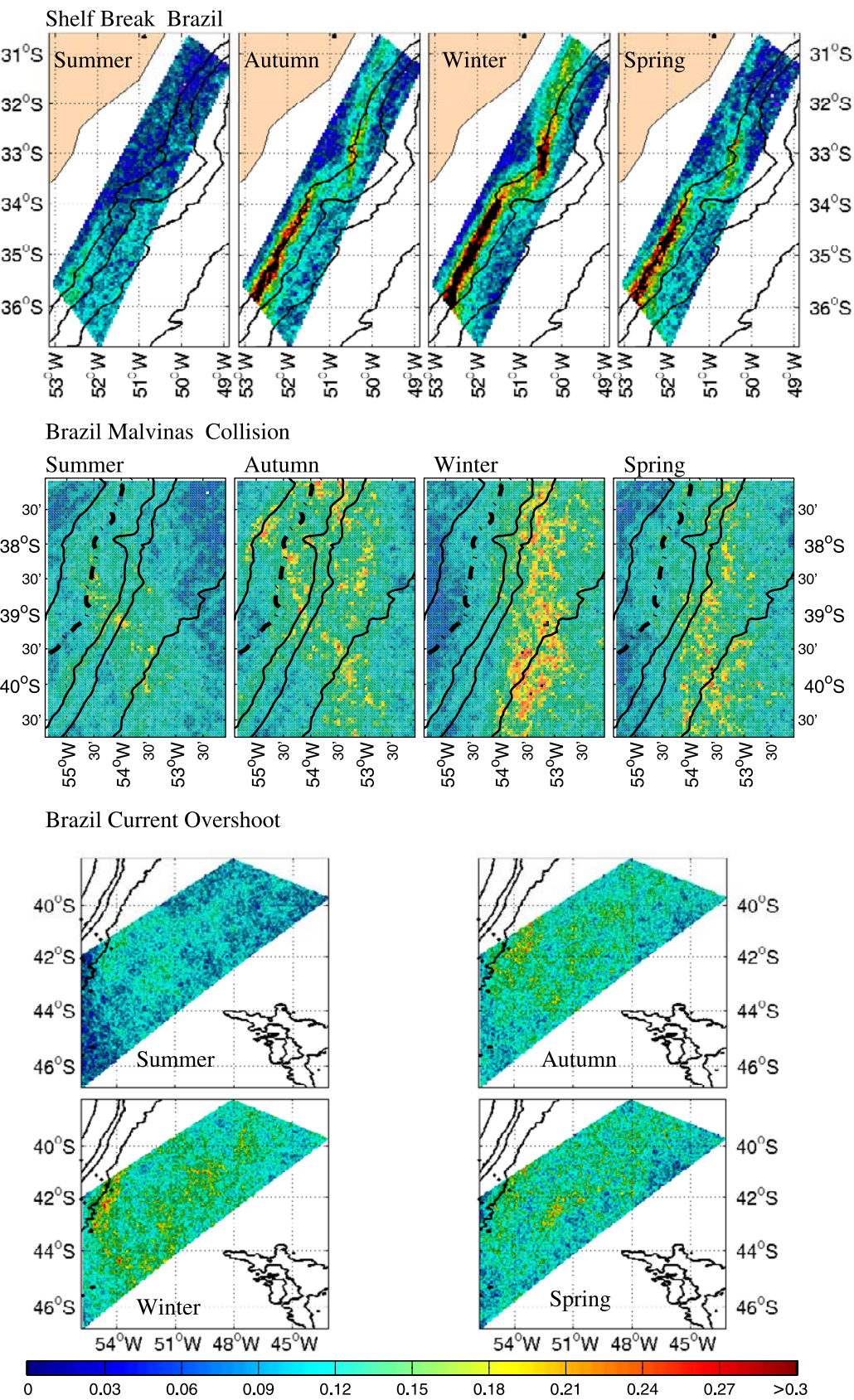
**Figure 6**

Figure 6. (top) Seasonal frontal probability distribution for the Shelf Break-Brazil region, (middle) Brazil Malvinas Collision region, and (bottom) Brazil Current Overshoot region. Solid black lines are the f/h contours indicated in Figure 3. Dash-dotted line in the BM-C region is the 1000 m isobath. The color bar indicates the frontal probability and is common for all panels.

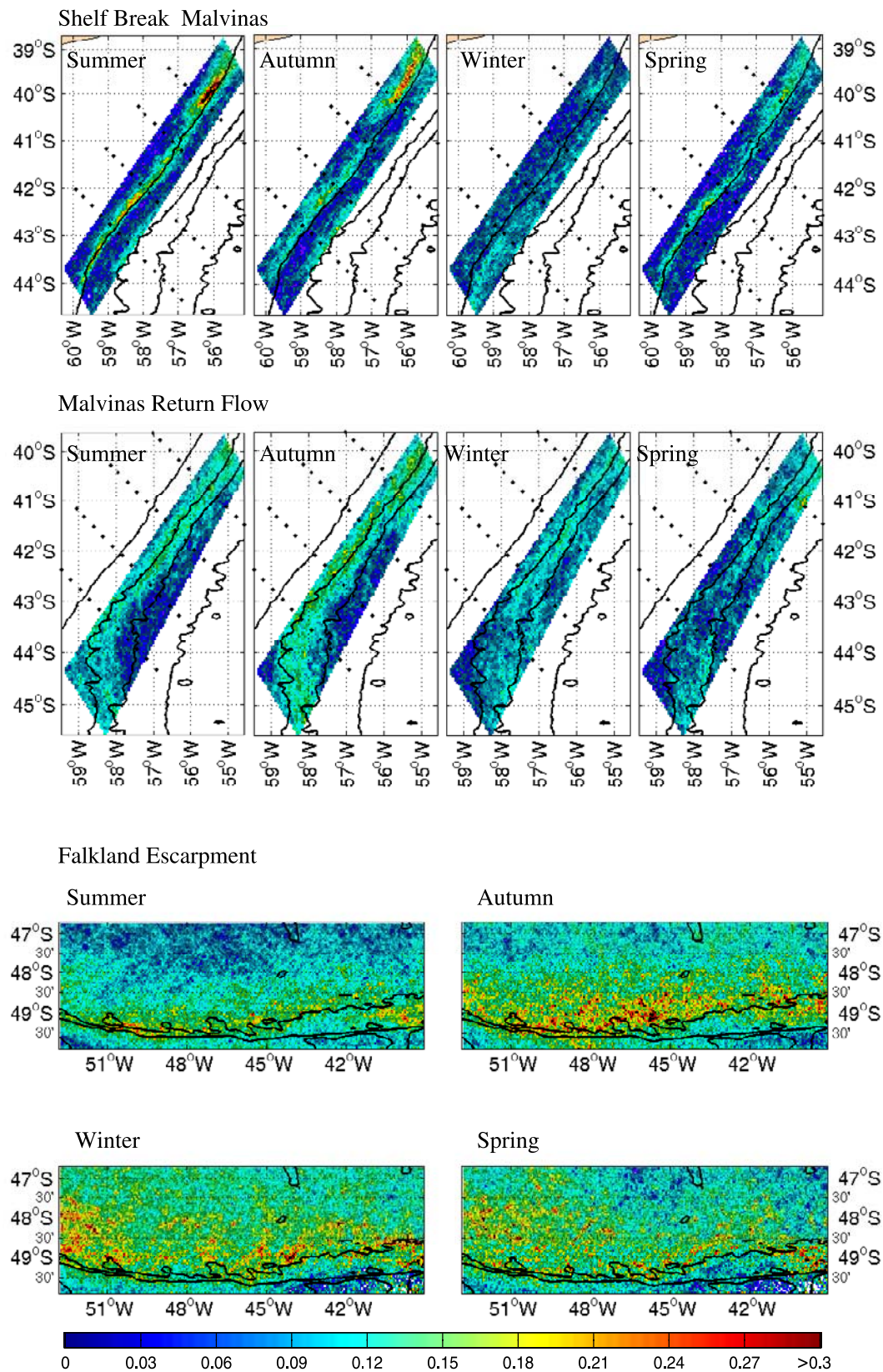
**Figure 9**

Figure 9. (top) Seasonal frontal probability distribution for the Shelf Break-Malvinas region, (middle) Malvinas Return Flow region, and (bottom) Falkland Escarpment region. Solid black lines are the f/h contours indicated in Figure 3. Dots in upper and middle panels indicate the locations selected to study the cross-front structure presented in Figure 11. On each section points are separated by ~ 30 km. The color bar indicates the frontal probability (and is common for all panels). Frontal probability values ranges from 0 to 1.